Research Article

Michael Stöger-Pollach*, Ze F. Scales, Leo Stöger, Firat Becer and Andreas Steiger-Thirsfeld

Advantages of low voltage electron microscopy in semiconductor research

https://doi.org/10.1515/mim-2025-0015
Received April 22, 2025; accepted November 3, 2025;
published online December 11, 2025

Abstract: Investigating semiconductors free of radiation damage on a sub-nanometer scale is essential for the development of modern semiconductor technologies. The robustness of such devices is often associated with chemical impurities that mainly decorate crystallographic lattice defects. Low voltage (scanning) transmission electron microscopy (LV-(S)TEM) combines all the analytical advantages of a (S)TEM with the fact that radiation damage is avoided. In addition, the optical properties can also be determined using valence electron energy loss spectrometry (VEELS), as relativistic energy losses can also be prevented. Using GaN we demonstrate the importance of the right choice of beam energy and discuss its influence on spatial resolution, since lattice defects are very localized. For GaN we find 60 keV to the best compromise between spatial resolution and damage free analytical investigations employing VEELS and cathodoluminescence (CL) without being altered by relativistic radiation emission, such as Čerenkov-radiation and its corresponding energy losses.

Keywords: beam energy; beam damage; optical properties; spatial resolution; cathodoluminescence; EELS

1 Introduction

The development of new semiconductor technologies also requires the development of better analytical techniques, because of constantly shrinking dimensions of semiconductor components. As early as 1965, Gordon E. Moore established the well-known Moore's law [1], which determines the density of components on integrated circuits over time into the future. Of course, extrapolation takes us to the limits of atomic dimensions, but it illustrates that the dimensions of semiconductor components must become smaller. The main consequence of the reduction in dimensions is that the defect density of the semiconductor materials plays an increasingly important role in the performance and their stability. The reason for this is that defects lead to defect states in the electronic structure of the semiconductor, which in turn lead to leakage currents or similar. In addition, the heating of the electronic components during operation promotes the diffusion of impurities, which accumulate at the defects in energetically favored positions. This also disrupts the electronic structure and sets off a chain reaction that leads to permanent damage to the semiconductor component over time. The best-known method of analyzing semiconductor structures in detail is transmission electron microscopy. The advantage here is that both imaging and analytical methods can be combined with a spatial resolution of just a few angstroms. This allows crystal defects to be characterized using electron diffraction. However, the strain fields that emanate from them can also be mapped. A Z-contrast image can also be generated using Rutherford-scattered electrons. All this information contributes to the understanding of semiconductors. The analytical possibilities of a (S)TEM include simple elemental maps recorded with energy dispersive X-ray spectrometry (EDX) or electron energy loss spectrometry (EELS) in scanning mode, energy filtered TEM imaging, energy loss near edge structure (ELNES) maps, plasmon maps, or even CL spectral maps with high spatial resolution.

However, whenever analytical methods are used, we have to ask ourselves whether artefacts caused by sample preparation or even bombardment with fast electrons are distorting the measurement results. This would result in the superimposition of artefacts with the signals of the pristine sample. The most sensitive method for visualizing radiation damage is CL. In the present work, we will therefore first determine the threshold energy of the electron beam

***Corresponding author: Michael Stöger-Pollach**, University Service Centre for TEM, TU Wien, Stadionallee 2, 1020 Vienna, Austria; and Inst. for Solid State Physics, TU Wien, Vienna, Austria,
E-mail: stoeger@ustem.tuwien.ac.at
Ze F. Scales, KAI GmbH, Villach, Austria
Leo Stöger, **Firat Becer and Andreas Steiger-Thirsfeld**, University Service Centre for TEM, TU Wien, Vienna, Austria

that must not be exceeded in order to avoid beam damage. Only then can we look at the other advantages of low beam energies for the experimental determination of band gaps or other optical properties. However, since lower beam energies also mean a longer wavelength of the electrons and thus a poorer spatial resolution, the aspect of spatial resolution is also discussed in detail. Finally, we measure the optical properties, the band gap and the chemical composition in dislocations in a GaN sample and compare these with stoichiometric GaN. Changes in the bandgap region are visualized using both EELS and CL.

2 Materials and methods

All CL experiments were carried out at room temperature in scanning mode employing an FEI TECNAI F20 with a high-brilliance field emission emitter, and high angle annular darkfield (HAADF) detector and a GATAN GIF Tridiem energy analyzer. The achievable spatial resolution is 1.36 Å in scanning mode. At a beam energy of 60 keV, still 3.9 Å can be realized. The CL system is a GATAN VULCAN CL recording and analyzing system consisting of a dedicated sample holder, light guides and a Czerny-Turner type spectrometer with a grating of 150 lines/mm. All EELS experiments were carried out on an FEI TECNAI G20 with a standard field emission emitter. This TEM is equipped with a GATAN GIF2001, which allows EELS spectra to be recorded at any beam energy between six and 200 keV. In order to obtain sufficient signal even at such extremely low energies, a scintillator was integrated into the camera that is thinner than the standard ones.

2.1 Beam damage

As already mentioned in the introduction, the most important limiting factor of any examination is the influence of the examination method on the result itself. It only fits if it can be ensured that the examination method does not falsify the result. In the case of electron microscopy, the damage to the sample caused by the fast electrons themselves must therefore be taken into account. For this purpose, we have examined a GaN/AlGaN layer structure (test sample 1) from industrial production prepared as focused ion beam –(FIB-) lamella with a lamella thickness of 150 nm. The advantage of the layer structure is that a particularly intense CL signal can be expected due to the confinement in the quantum walls and beam damage is therefore easier to quantify. Figure 1 shows (A) a panchromatic CL image and (B) the Bragg-contrast image of a buried AlGaN/GaN quantum well (QW) structure. The QWs appear as a bright band in the center of the panchromatic image, since it releases many more photons under electron beam irradiation as compared to stoichiometric GaN. Many threading dislocations can be observed in the Bragg-contrast STEM image, starting even below the QW structure.

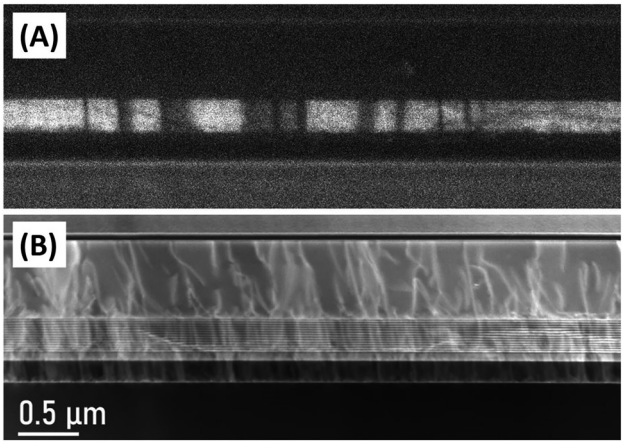

Figure 1: (A) Panchromatic CL image of a GaN/AlGaN quantum well test structure (bright band) after illumination lasting for 2 s with beam currents between 15.3 and 4.4 nA at beam energies between 80 keV and 200 keV. (B) Bragg contrast image recorded simultaneously with (A). No beam damage or contamination is visually detectable.

For studying the influence of beam current on sample damage, we varied the beam current between 15.3 nA and 4.4 nA at beam energies of 200 and 80 keV, respectively. In the panchromatic image the damaged areas appear as dark lines, since we scanned across the QW structure with 2 s exposure time per position and 30 positions on a line. It is remarkable, that absolutely no damage can be observed in the Bragg-contrast image using an annular dark filed (ADF) STEM detector. Visual inspection is not sufficient to judge whether beam damage happened or not. Consequently, the beam damage caused by electron irradiation in GaN can be related to point defects. Due to the high beam currents, all damaged lines are of large intensity reduction. Thus, it is not possible to distinguish between the different experimental conditions from Figure 1(B).

When changing the beam energy and again performing line scans across the QW structure with 2 s exposure time and 30 equidistant positions per line, but using a low beam current of 0.78 ± 0.06 nA for all energies, the damage threshold can be determined.

When measuring the reduction of the intensity, which is the contrast in the image, we can find out the damage threshold energy (see Figure 2). Our linear fit in Figure 2(B) gives a threshold value of 69.6 keV. This is in excellent agreement with [2]. An additional 60 keV STEM line scan with 9.76 nA beam current did also not show any reduction of the

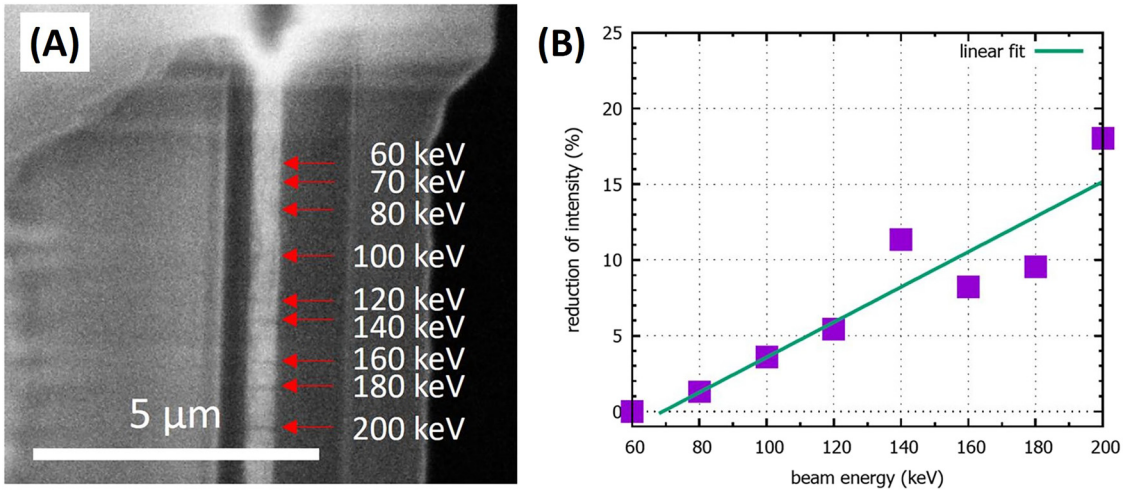

Figure 2: (A) Line scans with 2 s exposure time and constant beam currents of 0.8 ± 0.07 nA and beam energies between 60 keV and 200 keV. (B) Reduction of intensity in the panchromatic image as measure for defect creation. The linear fit starts at 69.6 keV, which is in perfect agreement with [2].

intensity in the panchromatic image. Thus, we can conclude, that below the damage threshold, the GaN is robust. Already earlier investigations [3] have shown, that even 80 keV electrons are preferable to 200 keV for the same reason.

2.2 Optical properties measured with VEELS

Electronic properties are of utmost interest in semiconductor research. When applying valence electron energy loss spectrometry (VEELS) access to the dielectric function ε is given. Beside the zero loss signal, the EELS spectrum is a self-convolution of the single scattering distribution (SSD(ω)), which itself is related to the dielectric function via the energy loss function Im(−1/ε(ω)), using $e\Delta E = \hbar\omega$. Here e is the electron charge, ΔE the energy loss, and ω the circular frequency.

$$\mathrm{SSD}(\omega) = \frac{2\pi e^2}{\pi^2\hbar^2 v^2} \cdot (I_0 t) \cdot \ln\left[1 + \left(\frac{\beta}{\vartheta_e}\right)^2\right] \cdot \mathrm{Im}\left(\frac{-1}{\varepsilon(\omega)}\right)$$

Here, ϑ_e is the characteristic scattering angle, β is the acceptance angle of the electron energy loss analyzer, t is the sample thickness, I_0 is the incoming intensity, and v is the speed of the probe electron. Since the SSD(ω) is related to the energy loss function, access to the whole dielectric function is given vie the Kramers-Kronig relations:

$$\mathrm{Re}\left(\frac{1}{\varepsilon(\omega)}\right) = 1 - \frac{2}{\pi} P \int_0^\infty \mathrm{Im}\left(\frac{-1}{\varepsilon(\omega)}\right) \frac{d\omega'}{\omega' - \omega}$$

Where P stands for the Cauchy principal part of the integral. In general, this works well unless no other reasons for energy losses in the valence electron regime appear. Unfortunately, for high beam energies the conditions for the emission of Čerenkov radiation is fulfilled. In this situation electrons are faster than the speed of light inside the sample ($v_e > c_n$), thus the electrons have to slow down and light is emitted. The Čerenkov consequently alters the VEELS spectrum and must be avoided by reducing the beam energy. For GaN, having a refractive index n of 2.36 the maximum beam energy can be calculated to b 53.14 keV. When using 60 keV the effect is still too weak to be measured [4]. Other effects altering the low loss spectrum are the presence of Transition radiation losses [5]. For semiconductors however, their influence is indeed rather small and can be neglected. The spatial resolution is limited by the extension of the Coulomb field of the swift probe electron, being called the inelastic delocalization. First discussed by Niels Bohr [6] as adiabatic criterion, theory and experiment were further developed [7] in aloof geometry considering only vacuum-matter interfaces, and is finally described for matter-matter interfaces by Archibald Howie [8]. In general, the long-range Coulomb field of a swift electron is able to provide enough power at a certain distance to excite valence electrons in the vicinity of the electron beam. Depending on the distance, more or less energy can be transferred to the excitation process, thus reducing the spatial resolution for lower energy losses.

Beside avoiding the excitation of Čerenkov losses, the inelastic scattering cross section increases with decreasing beam energies. Thus, the mean free path length for inelastic scattering processes λ shrinks. As a consequence, the relative sample thickness t/λ increases. Therefore, sample thicknesses of less than 80 nm are preferable. Using the data

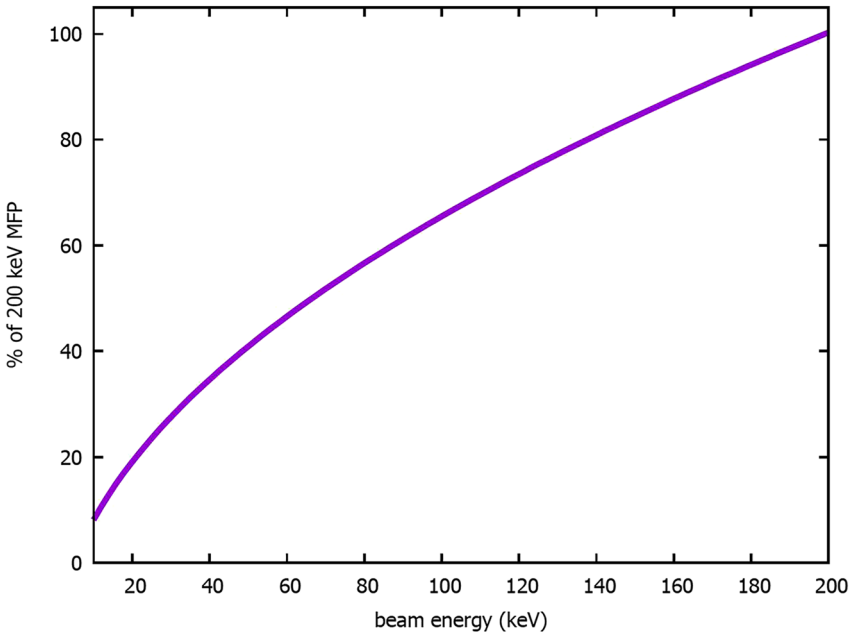

Figure 3: Universal curve for the reduction of the mean free path length. The MFP is given in percent of the one for 200 keV electrons.

published in [9], we calculate the relative mean free path length with respect to conventional 200 keV electron beams in the range from 10–200 keV. The curve follows a universal function for all materials with

$$\lambda(E_0) = \frac{a + b \cdot \sqrt{c \cdot E_0}}{\lambda(E_0 = 200keV)}$$

shown in Figure 3. The parameters *a, b, c* vary with respect to the material under investigation but are in the range of approximately $a = -24{,}31 \pm 4{,}02$, $b = 0.26 \pm 0.03$ and $c = 1.86 \pm 0.11$ considering the data for Al_2O_3, SiO_2, AlAs, AlN, GaN, GaP, and InAs, respectively.

The parameter *a* includes that for lower beam energies this behavior fits not anymore to real conditions. The MFP for many materials for 200 keV electrons can be found in [10].

2.3 Cathodoluminescence spectrometry in STEM

When recording optical spectra in electron microscopy, one has to distinguish between coherent and incoherent light emission [11]. The prior ones are directly related to the fact that a charge enters or travels through a medium, like Transition radiation or Čerenkov radiation, respectively, whereas the second is related to the de-excitation of an earlier excited electron. In this case, light is emitted, when a valence electron was excited into the conduction band and recombines with a hole in the valence band spontaneously and independent from the excitation process [12]. But the CL detection system itself cannot distinguish between photons being related to coherent or incoherent emission processes. If the optical properties of a sample are to be investigated, it must therefore be ensured that at least the incoherent photon emissions dominate during the experiment, or even that only these occur. Consequently, a reduction of beam energy is preferable. Additionally, since the inelastic scattering cross section also increases with decreasing beam energy, the light emission probability increases, thus leading to more CL signal or shorter recording times [13].

The spatial resolution of CL signal is not limited by the probe diameter, as it would be the case in STEM imaging or STEM-EELS analysis – here under consideration of the inelastic delocalization [7] – but it is related to the diffusion length of electrons and holes in combination with the relaxation time of the excited state.

2.4 Chemical quantification using EELS

In contrast to VEELS, where lower beam energies are favorable, chemical quantification works better when employing higher beam energies. The reason can again be found in the discussion about the mean free path lengths. A reduced MFP causes more multiple scattering events and thus in a worsened signal-to-background ratio at the positions of the ionization edges. The background is related to multiple plasmon scattering and is mathematically described as a multiple self-convolution of the SSD*(ω)* [14]. Under consideration of all the beforehand mentioned aspects, especially the one of beam damage, chemical quantification must be the last step in the overall quantification process.

3 Results

The object to be analyzed were dislocations in a GaN test specimen 2 (see Figure 4) and their influence on the optical properties of a GaN based semiconducting test structure. The sample thickness was 120 nm, being a compromise between VEELS and EELS on one hand and CL on the other hand, which are asking for thinner and thicker samples, respectively [15]. By using focused ion beam (FIB) a lamella was prepared. During the last milling steps, extreme care was taken not to damage the structure even in terms of the creation of point defects. Figure 4 shows a Z-contrast image recorded with 60 keV electrons by using the HAADF detector. A faint signal of Carbon contamination can be observed at the area, where the slow CL-map was recorded. Since the CL signal is most sensitive to any changes of the specimen caused by the beam-matter interaction, this map was recorded first on the pristine sample. EELS is less sensitive, thus it is recorded later on.

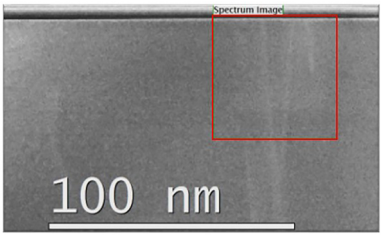

Figure 4: GaN test sample with dislocations. The red box gives the position of measurements for CL and VEELS studies at 60 keV beam energy as well as for 200 keV EELS studies for chemical quantification.

The brighter contrast at the position of the dislocations indicates a larger mean atomic number as compared to the surrounding matrix. Simultaneously VEELS and CL spectra were recorded using 60 keV beam energy, not to damage the sample and in order to avoid the appearance of the Čerenkov-effect altering both, the VEELS and CL spectra. From the VEELS spectra the onset of the signal caused by inelastically scattered electrons as well as the refractive index and other optical properties can be extracted. Figure 5 gives now an even better insight into the dislocations of interest. In Figure 5(A) the Bragg-contrast image shows the strain field surrounding the dislocations, Figure 5(B) is again the Z-contrast image recorded simultaneously with the VEELS and CL data sets (but with a 16×16 sub-pixel scanning routine during the acquisition of a single pixel in the CL and VEELS data sets). For analyzing small changes in the bandgap region, we deconvolved all spectra from zero-

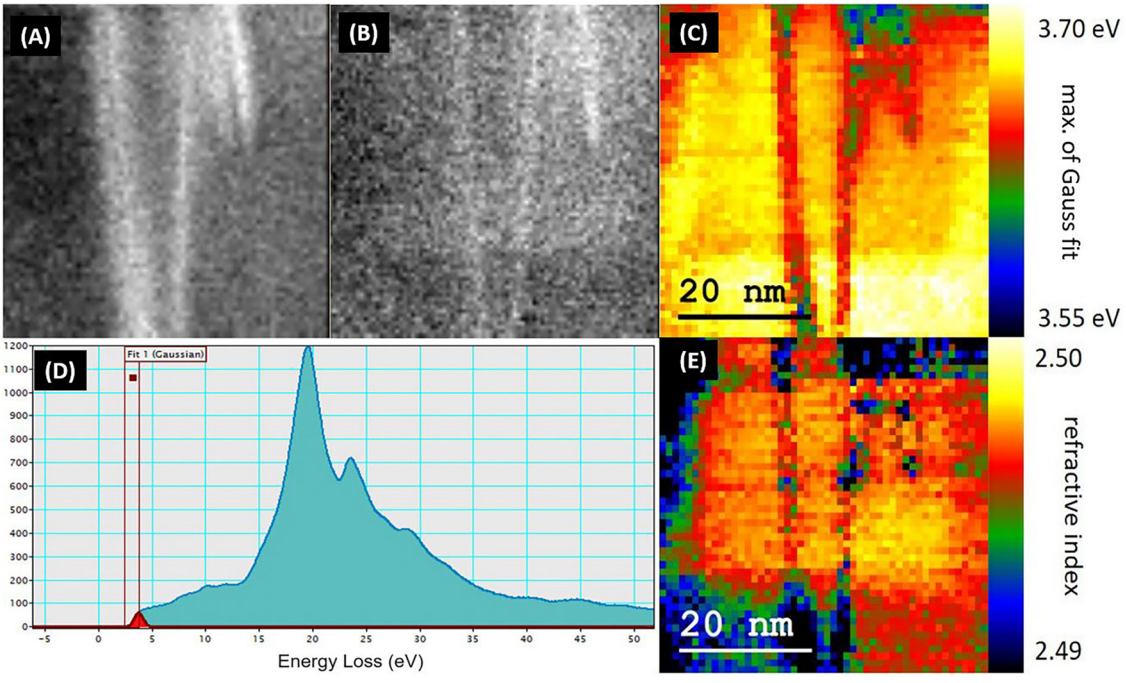

Figure 5: STEM-EELS investigation of dislocations. (A) Bragg-contrast image showing the strain fields surrounding the dislocations. (B) Z-contrast image with higher contrast for heavier elements. (C) Map showing the max. position of the Gaussian fit in the onset of the signal caused by inelastically scattered electrons deduced from the VEELS spectra after multiple scattering deconvolution and ZLP subtraction, (D) single scattering distribution of a VEELS experiment in the GaN matrix showing a Gaussian fit, and (E) refractive index map after KKA in each pixel of the 3D VEELS data set.

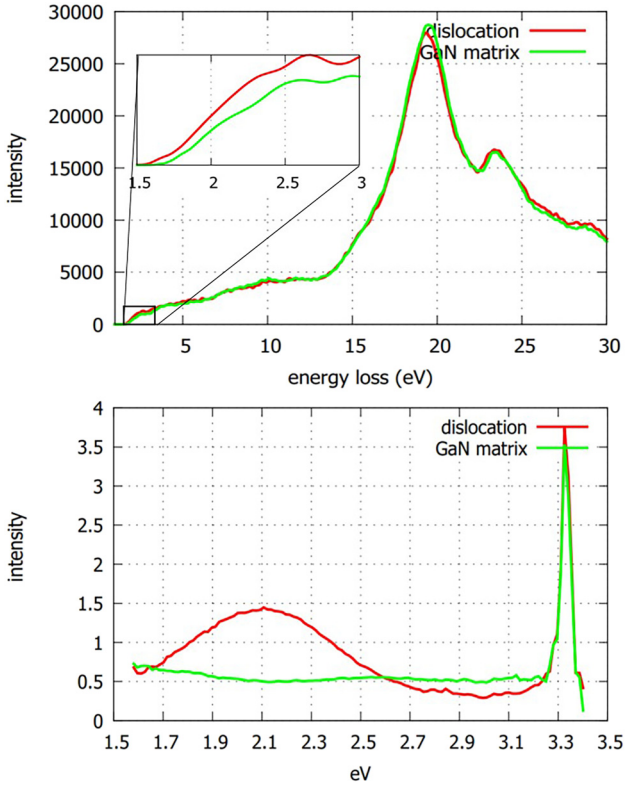

Figure 6: EELS (top) and CL (bottom) spectra recorded during the spectrum image acquisition shown in Figure 5. Six spectra were averaged in order to improve the signal-to-noise ratio even further. In both, VEELS and CL, additional intensity at around 2 eV can be detected.

and multiple scattering. Afterwards we fitted a Gaussian function into the onset of the inelastic signal (see Figure 5D). Since we allow the fit routine only to vary in height and position, but not in shape, the variation of the maximum of the Gaussian fit can be used as a quantitative value for changes in the bandgap region. This means, if we see a shift to lower beam energies, some gap-states or a bandgap reduction is present. Figure 5(C) gives the energy of the maximum of the Gaussian fit functions determined in each pixel after multiple scattering and zero loss [4]. The difference in the bandgap between the dislocation and the surrounding matrix is approximately 0.06 eV (red color vs. yellow color in Figure 5(C)), which is on one hand below the spectral resolution but on the other hand not below the spectral accuracy. Finally, in every spectrum Kramers-Kronig Analysis (KKA) was performed leading to the refractive index map shown in Figure 5(E).

Such a large set of data points also allows for statistical analyses. In the present situation, we performed principal component analysis (PCA) under strict observation of all components not included into the recombination routine. Observing the components not used anymore guarantees that indeed only noise is removed [16]. The reproducibility within the spectrum image – all spectra recorded at the positions of the dislocations show the same reduced bandgap and all spectra in the GaN matrix show another same bandgap – gives us confidence in correct data treatment. When looking at the VEELS and CL data in detail, one finds a similarity: at around 2 eV – which would be a yellow light emission – additional intensity can be detected. At 3.3 eV the main interband transition (MIBT) peak can be found in the CL spectra. Both, the VEELS and CL spectra are shown in Figure 6.

Finally, chemical analysis employing EELS is performed at an elevated beam energy of 200 keV. Figure 7 shows on

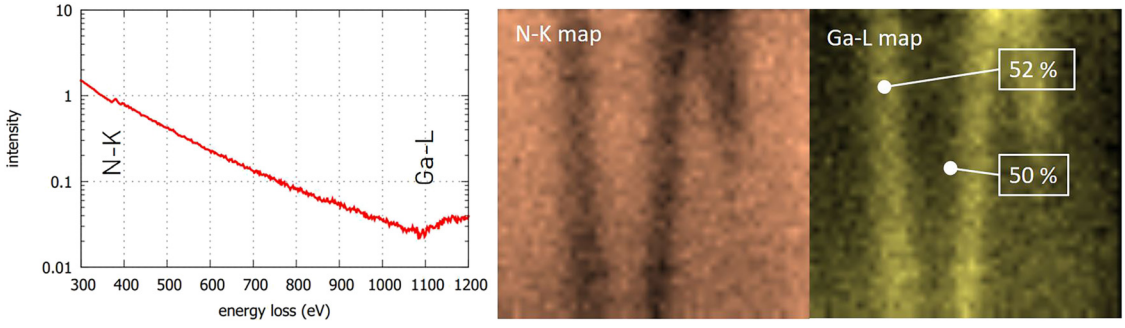

Figure 7: Left: 200 keV EELS spectrum of GaN in the energy range between 30 and 1,200 eV energy loss showing both, the N–K edge and the Ga-L_3 edge, respectively. Center: N–K map recorded in STEM-EELS mode, left: Ga-L map recorded simultaneously. The chemical quantification is shown only for the Ga-concentration.

the left hand side a single EELS spectrum out of the whole data set used for chemical quantification. On the right hand side two elemental maps for N and Ga, respectively, are shown. We find, that the dislocation is Ga-rich, which is also in perfect agreement with the Z-contrast image shown in Figure 5B.

4 Conclusions

In the present work, we discuss the advantage of low voltage electron microscopy for damage free investigations of semiconductors. We find that not for all applications low beam energies are preferable. However, because modern TEMs have a high degree of flexibility in terms of acceleration voltage, the optimum beam energy can be selected for each application. In the case of CL spectrometry, even point defects being invisible in the visual inspection of Bragg-contrast images are critical. Therefore, low beam energies must be selected for the first inspection and measurements of semiconductors. Additionally, low beam energies avoid the appearance of the Čerenkov effect, hence the CL and VEELS spectra are not altered. Finally, after all sensitive measurements were done, elevated beam energies might be used for further chemical analyses. In the present case study, we were able to identify the chemical and optical properties of defects in a GaN test structure using 60 keV electrons. We measure their bandgaps and refractive indices, find confidence by reproducibility between different positions of measurements but also because of employing different methods leading to the same results. Last but not least, chemical quantifications in the nm range confirm the previous findings.

Acknowledgments: The authors acknowledge TU Wien Bibliothek for financial support through its Open Access Funding Programme.
Research ethics: Not applicable.
Informed consent: Not applicable.
Author contributions: All authors have accepted responsibility for the entire content of this manuscript and approved its submission.
Use of Large Language Models, AI and Machine Learning Tools: None declared.
Conflict of interest: The author states no conflict of interest.
Research funding: None declared.
Data availability: Data will be made available on request.

References

[1] G. E. Moore, “Cramming more components onto integrated circuits,” *Electronics*, vol. 38, pp. 114—117, 1968. Publisher Item Identifier S 0018-9219(98)00753-1.
[2] J. T. Griffith *et al*., “Nano-cathodoluminescence reveals the effect of electron damage on the optical properties of nitride optoelectronics and the damage threshold,” *J. Appl. Phys.*, vol. 120, 165704, pp. 1—6, 2016, https://doi.org/10.1063/1.4965989.
[3] G. Schmidt *et al*, “Nano-scale luminescence characterization of individual InGaN/GaN quantum wells stacked in a microcavity using scanning transmission electron microscope cathodoluminescence,” *Appl. Phys. Lett.*, vol. 105, 032101, pp. 1—4, 2014, https://doi.org/10.1063/1.4890670.
[4] M. Stöger-Pollach, “Optical properties and bandgaps from low loss EELS: Pitfalls and solutions,” *Micron*, vol. 39, no. 8, pp. 1092—1110, 2008.
[5] M. Stöger-Pollach, L. Kachtík, B. Miesenberger, and P. Retzl, “Transition radiation in EELS and cathodoluminescence,” *Ultramicroscopy*, vol. 173, pp. 31—35, 2017.
[6] N. Bohr, “On the theory of the decrease of velocity of moving electrified particles on passing through matter,” *Phil. Mag.*, vol. 25, no. 145, pp. 10—31, 1913.
[7] D. A. Muller and J. Silcox, “Delocalization in inelastic scattering,” *Ultramicroscopy*, vol. 59, no. 1—4, pp. 195—213, 1995.
[8] A. Howie, “Valence excitations in electron microscopy: Resolved and unresolved issues,” *Micron*, vol. 34, no. 3—5, pp. 121—125, 2003.
[9] H. Shinotsuka, S. Tanuma, C. J. Powell, and D. R. Penn, “Calculations of electron inelastic mean free paths. XII. Data for 42 inorganic compounds over the 50 eV to 200 keV range with the full Penn algorithm,” *Surf. Int. Analysis*, vol. 51, no. 4, pp. 427—457, 2018.
[10] K. Iakoubovskii, K. Mitsuishi, Y. Nakayama, and K. Furuya, “Mean free path of inelastic electron scattering in elemental solids and oxides using transmission electron microscopy: Atomic number dependent oscillatory behavior,” *Phys. Rev. B*, vol. 77, 104102, pp. 1—7, 2008, https://doi.org/10.1103/PhysRevB.77.104102.
[11] F. J. García de Abajo, “Optical excitation in electron microscopy,” *Rev. Mod. Phys.*, vol. 82, no. 1, pp. 210—275, 2010.
[12] M. Stöger-Pollach *et al*., “Coherent light emission in cathodoluminescence when using GaAs in a scanning (transmission) electron microscopy,” *Ultramicroscopy*, vol. 224, 113260, pp. 1—6, 2021, https://doi.org/10.1016/j.ultramic.2021.113260.
[13] M. Kociak and L. F. Zagonel, “Cathodoluminescence in the scanning transmission electron microscope,” *Ultramicroscopy*, vol. 176, pp. 112—131, 2017.
[14] R. F. Egerton, “Electron energy-loss spectroscopy in the TEM,” *Rep. Prog. Phys.*, vol. 72, 016502, pp. 1—25, 2009, https://doi.org/10.1088/0034-4885/72/1/016502.
[15] K. Pantzas, *et al*., “Role of compositional fluctuations and their suppression on the strain and luminescence of InGaN alloys,” *J. of Applied Physics*, vol. 117, no. 5, 2015, Art no. 055705.
[16] P. Potapov, “On the loss of information on PCA of spectrum-images,” *Ultramicroscopy*, vol. 182, pp. 191—194, 2017.